

The use of vibrational spectroscopy to study the pathogenesis multiple sclerosis and other neurological conditions

RAMOS, Ines <<http://orcid.org/0000-0002-0142-1224>>, LYNG, Fiona M., REHMAN, Ihtesham Ur, SHARRACK, Basil and WOODROOFE, Nicola <<http://orcid.org/0000-0002-8818-331X>>

Available from Sheffield Hallam University Research Archive (SHURA) at:
<https://shura.shu.ac.uk/16203/>

This document is the Accepted Version [AM]

Citation:

RAMOS, Ines, LYNG, Fiona M., REHMAN, Ihtesham Ur, SHARRACK, Basil and WOODROOFE, Nicola (2017). The use of vibrational spectroscopy to study the pathogenesis multiple sclerosis and other neurological conditions. *Applied Spectroscopy Reviews*, 52. [Article]

Copyright and re-use policy

See <http://shura.shu.ac.uk/information.html>

The use of vibrational spectroscopy to study the pathogenesis multiple sclerosis and other neurological conditions

Inês R. Ramos^a, Fiona M. Lyng^b, Ihtesham Ur Rehman^c, Basil Sharrack^{d,e} & M.

Nicola Woodroffe^a

^aBiomolecular Sciences Research Centre, Faculty of Health and Wellbeing, Sheffield Hallam University, Sheffield, UK; ^bDIT Centre for Radiation and Environmental Science, Focas Research Institute, Dublin Institute of Technology, Dublin, Ireland; ^cDepartment of Materials Science and Engineering, The Kroto Research Institute, Sheffield, UK; ^dSheffield Teaching Hospital Foundation Trust, Academic Department of Neurology; ^eThe University of Sheffield, Sheffield Institute for Translational Neuroscience and the Sheffield NIHR Biomedical Research Centre for Translational Neuroscience.

CORRESPONDING AUTHOR: Inês R. Ramos I.Ramos@shu.ac.uk Biomolecular Sciences Research Centre, Faculty of Health and Wellbeing, Sheffield Hallam University, Owen Building, City Campus, Howard Street, Sheffield, S1 1WB, UK.

RUNNING HEAD: Spectroscopy for multiple sclerosis

KEYWORDS: Multiple sclerosis, normal-appearing white matter, pathology, spectroscopy

1 **Abstract**

2 Spectroscopy techniques are valuable tools in biomedical research and have been used
3 extensively in the study of disease. However, neurological conditions such as multiple
4 sclerosis (MS) have received little attention and the available spectroscopy studies are
5 limited, both in overall numbers of patients studied and the disease samples considered. MS
6 is a complex immune-mediated disease, with variable clinical courses and limited
7 therapeutic options. This review aims to summarize current literature in the area,
8 demonstrating how spectroscopy techniques can provide valuable information to inform and
9 advance research into the most common neurological condition affecting young adults.

Introduction

Biophotonic techniques are now widely used in biomedical research targeting better diagnosis, prognosis and surveillance of disease. Vibrational spectroscopy methods such as Fourier-transform infrared (FTIR) and Raman spectroscopy are so called because they probe the intramolecular vibrations and rotations of a sample when irradiated with a light source (1). The vibrational energy levels can be probed by both techniques, using different physical processes. Raman spectroscopy studies the Raman effect, the spontaneous inelastic light scattering process of photons, following the interaction of monochromatic radiation (e.g. a laser) with the sample. In contrast, FTIR spectroscopy studies the samples' absorption characteristics arising from the molecular motion due to atomic displacement upon interaction with an infrared source (2, 3). In both cases, the recording of vibrational energy level transactions results in a spectrum composed of peaks/bands that can be interpreted qualitatively (peak position) and quantitatively (peak intensity/area) (4). In FTIR spectroscopy, the spectral bands arise from a change in the electric dipole moment of the molecules, whereas in Raman spectroscopy, they arise from a change in molecular polarizability. FTIR and Raman spectroscopies are therefore complementary and provide a "fingerprint" or "signature" of the specific molecules contained within a biological sample (proteins, lipids, DNA), depending upon whether their bonds exhibit infrared or Raman activities. Both FTIR and Raman can be used for imaging tissue sections and are non-destructive, label-free techniques with sub-micron spatial resolution (5).

In biomedical research, scientists are continually investigating and exploring the application of new technologies that can detect early signs of disease and thereby reduce disease morbidity and mortality. The detection of biomarkers plays an important role in this exploration. In oncology, such biomarkers, have been used extensively to determine risk factors, aid diagnosis and prognosis, and in the assessment of treatment response as well as determining disease recurrence (4). However, from amongst the vast numbers of candidate biomarkers, only a limited few have been validated for clinical use. Vibrational spectroscopy is new investigatory tool in biomarker (re)search which is not restricted to the analysis of a specific protein, nucleic acid and/or lipid. As such, FTIR and Raman spectra are able to give spectral "signatures" or "biomarkers" which reflect the overall molecular composition of the studied samples (4).

Despite being extensively used in the field of cancer research (6, 7), FTIR and Raman spectroscopy are currently under explored in the study of diseases which affect the central nervous system (CNS) including multiple sclerosis (MS). To date, there are very few published papers in this field including a review article published in 2012 (8).

Multiple Sclerosis (MS)

MS is considered to be an autoimmune, neuro-inflammatory and degenerative condition, which affects both the brain and spinal cord. Its precise aetiology remains unknown, although both genetic and environmental factors influence an individual's susceptibility to develop MS (9). The clinical course of this disease is variable but is divided into several categories reflecting the degree of clinical disease activity and disability progression rate, including relapsing remitting (RRMS), primary progressive (PPMS) and secondary progressive MS (SPMS) (10). Whilst the inflammatory component of MS pathogenesis is relatively well understood, the progressive neurodegenerative component of the disease, in both its primary and secondary progressive clinical courses, is yet to be elucidated. In PPMS, patients have a gradual and progressive decline in function from the outset, with minimal disease activity detectable on magnetic resonance imaging (MRI) whereas in SPMS, the gradual progression follows an initial relapsing remitting phase, usually over many years (11). The consensus is that MS is a spectrum of conditions with RRMS being one end of that spectrum and PPMS being at the other.

The key pathological features observed in MS are the influx of inflammatory immune cells across the blood brain barrier into the CNS which results in the loss of axons and their insulating myelin sheaths and the formation of lesions (plaques) in the white matter (WM) and to a lesser extent in the grey matter (12). This process results in the impairment of conduction along the affected axon leading to variable symptoms experienced by affected patients including cognitive impairment, visual disturbances, sensory and motor symptoms, impaired balance, sphincter disturbance and fatigue (13). Histopathological comparisons of CNS tissue shows that the classical perivascular inflammation seen in SPMS is much less prominent in PPMS and that more diffuse inflammatory changes and greater extent of axonal damage in the normal appearing white matter (NAWM) are seen in PPMS (14, 15). In addition, there is evidence that patients with PPMS have a reduced capacity for remyelination (11). Understanding the underlying pathogenesis which underpins the clinical progression in MS at the molecular and cellular levels is therefore vital for the development of therapies targeting the neurodegenerative process and enhancing remyelination strategies.

The diagnosis of MS is usually based on the clinical presentation and the results of brain and spinal MRI, which reveals evidence of active and chronic lesions as well as focal and generalised atrophy (16). Current treatments for MS target the initial relapsing phase of the disease, by preventing inflammatory responses leading to a reduction in the number and severity of relapses (17). However, there are currently no treatments for primary and

secondary progressive MS although two therapeutic agents are waiting to be licenced (18). . The underlying pathogenesis of the initial inflammatory phase of MS has been well characterised at both the cellular and molecular level. However the pathogenesis of the progressive phase is still not fully elucidated, although changes in the NAWM appear to be pivotal (12). The progressive loss of axons seem to continues despite the reduction of relapses with the use of effective anti-inflammatory therapies resulting in irreversible disability which support the presence of two separate pathological processes: inflammation and neurodegeneration (19).

Approaches to studying MS pathogenesis have focussed on the analysis of post-mortem CNS tissue, as well as experimental work using both primary CNS cells such as astrocytes, microglia and oligodendrocytes isolated from CNS tissue, which allows manipulation of the individual cell's environment. In addition, a number of animal models of MS have been developed, primarily in rodents but also in primates, in order to investigate the disease course of MS. In these animals, experimental autoimmune encephalomyelitis (EAE) is induced through the injection of spinal cord homogenates, myelin proteins or peptides, such as myelin oligodendrocyte glycoprotein (MOG), myelin basic protein (MBP) or proteolipid protein (PLP), in addition to adjuvant. This promotes the induction of an autoimmune response against myelin, leading to both an inflammatory response in the CNS as well as, dependent on the model used, demyelination (20). Nevertheless, the progressive aspects of the human condition seen in MS are more difficult to reproduce in animal models (21), although Peferoen has recently described an EAE model in Biozzi mice which, dependent on the age of the mouse at induction of disease, demonstrates progressive disease, with younger mice having an initial relapsing remitting phase followed by a secondary progressive phase and older mice showing progression at onset of disease induction (22). A further drawback of these animal models is that off the multitude of therapies found to be effective in preventing EAE, a very small number have been taken forward into clinical trials (23), suggesting that the models do not fully mimic the pathogenesis of MS in humans.

Current research approaches to investigating the aetiology of MS focus on the search for specific genes/proteins/lipids that are thought to be involved in the disease process using a variety of cell and molecular biology approaches. More recently DNA microarrays have been used to assess more global changes in gene expression in MS diseased human CNS tissue compared with normal age matched control (24, 25). The application of proteomic and metabolomic analyses in MS have focussed on biomarkers in biological fluids, including blood, cerebrospinal fluid and urine rather than in MS CNS tissue (26, 27).

The advantage of Raman and FTIR for analysis of human tissues is that the overall chemical composition of the tissue in terms of lipids, nucleic acids and proteins is obtained. Spectroscopic study of MS has been reported in the literature using both human post-mortem CNS tissue and animal models of the disease. A review of all available original research articles published to date is provided below and is summarized in Table 1.

Human CNS tissue spectroscopy studies

Initial studies applying spectroscopic techniques to the study of MS pathology were reported in the 1990s. Choo *et al.* were the first to use FTIR to study human white and grey matter tissue, obtained from healthy control subjects, and compared it with MS demyelinated lesions tissue from MS patients (28). This rapid communication reported that it was possible to discriminate between different types of MS tissue attributed to variations in intrinsic lipid and water content. Whilst FTIR spectra of white matter was dominated by lipids and protein absorptions and grey matter spectra showed reduced lipid content alongside an increase contribution of water to the spectra; MS lesion spectra were suggestive of both lipid and water depletion, as would be expected from histopathological tissue analysis (28).

Differences comparing white and grey matter as well as white matter with MS lesions were most notable in the 2800-3000 cm^{-1} spectral region, where most infrared bands arise from CH_2 and CH_3 stretching vibrations of lipid acyl chains. Four main assignments were made to CH_3 and CH_2 asymmetric stretching vibrations at 2956 and 2922 cm^{-1} and, to symmetric vibrations at 2871 and 2851 cm^{-1} respectively. The overall intensity of these peaks were reduced in both grey matter and MS lesion tissue, compared to normal control white matter, which the authors explained was due to the expected lower lipid content of grey matter and MS lesions, due to demyelination. Similarly, the CH_2/CH_3 ratio is also decreased as a decrease in lipid to protein ratio leads to methylene and methyl groups of amino-acid side chains dominating this spectral region; as the CH_2/CH_3 ratio in proteins is much lower than in lipids, it was expected that the overall ratio would be decreased and band broadening would be observed. In order to distinguish between grey matter and MS lesion tissue, the authors reported the spectral region of 1200-1800 cm^{-1} to be most useful (28).

The main feature in white matter' spectra was observed at 1467 cm^{-1} and assigned to the scissoring vibration of CH_2 groups of lipid acyl chains. In grey matter, the intensity absorption of this CH_2 scissoring is reduced and is almost equal to the CH_3 asymmetric bending vibrations at 1456 cm^{-1} . This is explained by the reduction in lipid content, which is also

apparent by the decrease in intensity of the terminal methyl groups of lipid chains and of the $(\text{CH}_3)_3\text{N}^+$ symmetric bending of phosphatidylcholine headgroups, assigned to the bands at 1381 and 1415 cm^{-1} , respectively. In contrast the COO^- symmetric stretching band at 1400 cm^{-1} is increased in the spectra of grey matter in comparison to white matter. The same was also observed at 1308 cm^{-1} which the authors assigned to amide III(28).

The spectral features of MS plaque tissue are similar to the ones described for grey matter. Nevertheless, the intensity of CH_2 scissoring (1467 cm^{-1}) to CH_3 asymmetric bending vibrations (1456 cm^{-1}) is now reversed with CH_3 asymmetric bending vibrations being the main feature in this region. Similarly, the PO_2^- antisymmetric stretching band also displays greater intensity in the plaques' spectra comparatively to grey matter. Both these observations were suggested to indicate that lipid content of MS plaques is lower than that of the grey matter (28), which is known to be the case from histopathology studies (13).

In the 1500 to 11800 cm^{-1} spectral range the main feature observed was the amide I band which arises from the $\text{C}=\text{O}$ stretching vibration of amide groups of proteins and is centred at 1653 cm^{-1} . Other absorptions reported were assigned to C-C stretching of tyrosine at 1517 cm^{-1} ; the amide II band centred at 1550 cm^{-1} ; and the acidic amino-acid and arginine side chains at 1581 and 1580-1610 cm^{-1} respectively. In addition, the ratio of amide I to amide II was increased comparatively to that of isolated proteins. It was suggested this may result from non-protein contributions to the amide I region, and further proposing water to be the main source of this contribution (28).

Le Vine *et al.* (1998) assessed active lesions in MS tissue compared with healthy control white matter and reported an increased oxidation state of both lipids and proteins in MS lesions, indicative of a role for free radicals in MS pathogenesis (29). The spectra of WM tissue from control post-mortem cases was dominated by CH_2 absorptions at 2923 and 1468 cm^{-1} , $\text{P}=\text{O}$ at 1235 cm^{-1} and $\text{HO}-\text{C}-\text{H}$ at 1060 cm^{-1} , characteristic of lipids, phospholipids and glycolipids respectively. Areas of NAWM within MS cases were reported to display similar spectra to normal control white matter, whereas lesion areas display significant changes, such as a reduced ratio of CH_2 to NH and OH , in comparison with control white matter. Further differences were revealed by the investigation of the oxidation products of lipids and proteins. Previous studies reported the amide I peak at $\sim 1660 \text{ cm}^{-1}$ to be broader when proteins are oxidised and the carbonyl absorption at 1740 cm^{-1} to be increased when lipids are oxidised. This study reported the $\text{C}=\text{O}$ (1740 cm^{-1}) to CH_2 (1468 cm^{-1}) ratio to be increased and the peak at 1657 cm^{-1} to be broader in MS lesions in comparison with white matter from control samples (29).

Furthermore, the authors followed the spatial spectroscopic profiles of these features by recording linear maps acquired partially or wholly within MS lesions sites and representative areas of control white matter. They reported the CH₂ (1468 cm⁻¹) to amide II (1544 cm⁻¹) ratio to be 0.644±0.053 for control samples (n=5), ranging from less than 0.1 to 0.7 in MS ones (n=5); 15.950±1.593 was the mean of the C=O (1740 cm⁻¹) to amide II (1544 cm⁻¹) ratio in control cases, which was in turn decreased for all MS cases; and four out of five MS cases presented one or more values above the mean of 24.047±3.22 for C=O (1740 cm⁻¹) to CH₂ (1468 cm⁻¹) ratio of control samples. Finally, whilst controls displayed an average of -0.033±0.010 at 1652 cm⁻¹, MS cases displayed greater values all above -0.02 (29).

It was concluded that the higher carbonyl to CH₂ ratio detected in the spectra of MS cases is suggestive of lipids being oxidised, whilst oxidation of proteins cause the 1657 cm⁻¹ peak to broaden to 1652 cm⁻¹ in MS plaque tissue. This result may be caused by gliosis, which occurs in parallel with the demyelination process leading to higher expression of glial fibrillary acidic protein by astrocytes, which was also indicated as a potential factor contributing to the amide I broadening, as well as the relative greater expression of amide II (29).

More recently, Poon *et al.* used Coherent Anti-Stokes Raman Scattering (CARS) to study several regions of post-mortem MS brain, including areas of NAWM, remyelination and both active and chronic lesions (30). Investigating five chronic MS cases, they reported a novel instrument that allows acquisition of high resolution, label-free imaging whose pixels contain spectral information, together with a post-processing method, which allows isolation and quantification of these spectral images. The study showed the CH₂ symmetric stretch of 2850 cm⁻¹ in NAWM, to shift to 2885 cm⁻¹ when myelin was contained within the phagocytic macrophages/microglia cells within the tissue (a CARS image is overlaid with immunostaining with the marker HLA-DR/LN3, confirming activated microglia). This was proposed to arise from the intermolecular chain disorder resulting from the breakdown of the myelin components during demyelination. Further CARS pseudo-colour images showed myelinated axons to have greatly reduced density within remyelinated areas in active lesion sites (30).

An additional study, also by Poon *et al.* reported lipid biochemical changes preceding myelin protein loss in peri-lesional areas and NAWM, when inspecting the CH spectral region from 2750 to 3100 cm⁻¹ (31). CARS images were acquired from the NAWM region adjacent to the lesion and sequential images were acquired moving away from the lesion into the NAWM.. Triplicate images were also acquired from an area furthest away from the lesion site, referred to as "true NAWM" and from matched brain regions in tissue sections from control

non-MS cases. The average "true NAWM" spectra did not overlap with region-matched control spectra, suggesting possible underlying pathology in MS tissue, which is not differentiated when using lipophilic histochemistry or immunostaining with conventional techniques (31).

The three major features in the CH spectral region analysed, correspond to the symmetric and asymmetric and asymmetric stretching of acyl chain methylene at 2850 and 2886 cm^{-1} respectively, and the CH_3 methyl chain end symmetric stretch at 2935 cm^{-1} , which is thought to include protein contributions as well. Observing the intensity ratios of 2850/2880 cm^{-1} and 2935/2880 cm^{-1} the authors noted a slowing decreasing trend across all measured intensity ratios, when moving away from the lesion site until reaching the "true NAWM" ratios, recorded from an area the furthest away from the lesion, and approaching the ratios of region-matched non-MS control samples. The 2850/2880 cm^{-1} ratio is thought to relate to the intermolecular packing, interchain interactions and intrachain torsional motions, whereas the 2935/2880 cm^{-1} ratio allows monitoring intramolecular chain disorder and trans-gauche isomerisation. The authors conclude that biochemistry of myelin lipid content changes in the lesion periphery and in NAWM (31).

Mouse models of demyelination and remyelination

Animal models of MS have also been investigated by vibrational spectroscopy, where most studies aim to elucidate the mechanisms behind demyelination and remyelination. Heraud *et al.* used FTIR spectroscopy to investigate macromolecular components and protein conformational changes in the CNS of EAE versus control tissue sections(32). Using principal component analysis (PCA) and artificial neuronal networks (ANN) to analyse single data acquisition spectra, the authors demonstrated, without the need for chemical stains, subtle chemical and structural changes, particularly in the secondary structure of proteins in the white matter (33).

Fu *et al.* used resonant CARS imaging from the symmetric CH_2 stretch vibration at 2840 cm^{-1} to characterize myelin changes induced by lysophosphatidyl choline (lyso-PtCho) (34). Although not directly relevant to demyelinating diseases including MS, the authors reported CARS was able to characterise the changes occurring in lyso-PtdCho-induced myelin breakdown and that together with electrophysiological data, it revealed involvement of a Ca^{2+} , calpain, and cPLA₂-dependent pathway (34).

In another study, CARS was used to study myelin loss in the mouse-model, Relapsing-EAE (R-EAE) (35). Two theories have been hypothesised for initiating demyelination, one where

the injury starts at internodal myelin, thinning layer by layer and the other, where it initiates with paranodal domain injury. The authors noted that the submicron spatial resolution of CARS images allowed not only the quantification of myelin thickness but also the ratio of myelin thickness to the axonal diameter at different stages of the disease process. Furthermore, two-photon immunofluorescence microscopy revealed that juxtaparanodal K⁺ channels, paranodal myelin retraction and the displacement of K⁺ channels was extensively observed at the onset of R-EAE and at lesion borders. Overall their results suggested loss of nodal integrity precedes the formation of myelin debris in the CD4⁺ T-cell-mediated R-EAE model of MS and that remyelination is accompanied by reestablishment of the nodal makers, with myelin being only partially restored (35).

Furthermore, the Raman spectra of myelin were dominated by lipid assignments and the authors studied both C-C and C-H vibrational bands to determine the conformation of their hydrocarbon chains through: (1) lipid packing studied using prominent bands at 2850, 2885 and 2930 cm⁻¹, assigned respectively to stretching and asymmetric stretching of CH₂ and to CH₃ stretching; and, (2) lipid unsaturation using the ¹1650/¹1445 ratio, which represents the C=C stretching bands to H-C-H deformation bands in lipid acyl chains. Myelin debris presented a higher intensity of the ¹2930/¹2885 ratio, reflecting an increased intermolecular chain disorder; and regenerated myelin presented a higher lipid-packing disorder than normal myelin. Similarly, myelin debris presented the highest unsaturation degree, which was decreased in regenerated myelin but nevertheless was higher than normal myelin. Finally, the analysis of the ¹1122/¹1076 ratio, revealed no significant change could be observed in the intramolecular chain ordering of myelin debris, normal and regenerated myelin (35).

A non-invasive multimodal CARS system, combining reflectance for visualizing axons, fluorescence to visualize green fluorescence protein (GFP) and Raman to visualize myelin and to monitor microglia induced neurodegeneration was reported by Imitola *et al.* (36). Using an EAE model, the authors reported fast *ex vivo* imaging of myelin, axons and microglia with great anatomical precision in live tissue. CARS images showed a global decrease in myelination, not seen before through other imaging techniques. This suggests that subtle alterations in the myelin lipid content may precede hallmark CNS demyelination, which is correlated with axonal loss and microglia activation (36).

Wang *et al.* reported DBT (3,3'-diethylthiatricarbocyanine iodide) to be a promising probe for Near Infrared Fluorescence (NIRF) imaging of myelination (37). Through *in vivo* NIRF studies on hyper and hypomyelination mouse models, the authors demonstrated DBT successfully enters the brain and selectively binds to myelin sheaths. Furthermore, aiming to

broaden NIRF-DBT imaging to MS disease, the authors studied a cuprizone-induced mouse model for demyelination and remyelination. NIRF imaging and quantitative analysis revealed DBT could successfully monitor the level of demyelination and subsequent remyelination in this mouse model, that could be correlated with histochemical staining (37).

Future research directions

The current literature, as reviewed above, considering human post-mortem CNS tissue specimens is limited, with most studies considering a nominal sample number as shown in Table 1, which also summarises the studies completed in models of MS.

Studies focusing on animal models have shown spectroscopy to be a valuable tool in probing the biochemical composition of samples otherwise deemed identical. The spectral imaging of myelinating and remyelinating processes, for example, further demonstrated the ability to differentiate between newly formed myelin and endogenous myelin, indicating the remyelinating process generates myelin of a different composition. Nonetheless, studies considering human samples are limited and concern only a small number of post-mortem tissues as human CNS material is difficult to obtain. Furthermore, most studies focused on the spectral distinction of MS lesions from control tissue of non-diseased subjects, which can readily be achieved by macro and microscopic evaluation using luxol-fast blue (LFB) stain or immunohistochemistry for myelin proteins to examine demyelination. As disease diagnosis through tissue sampling is not feasible, the advantages of spectroscopy techniques such as FTIR and Raman rely on their ability to reveal underlying biochemical changes not yet detectable either macro or microscopically, for example on NAWM of MS cases, when common techniques fail to recognize differences. Spectral data could potentially help to understand the underpinning mechanisms of disease and advance research in the field by probing deeper into the chemical composition of apparently normal areas of MS cases.

FTIR and Raman spectroscopy analysis of post-mortem white matter MS tissue: NAWM has a different signature

Analysing four post-mortem brain samples obtained from UK MS Society Tissue Bank (Imperial College London) we show FTIR signatures allow the distinction of normal control WM from both active and chronic lesions, and more interestingly from the NAWM of MS cases despite no visible demyelination being observed when staining NAWM with LFB. The mean FTIR spectra of a brain tissue sample from control, NAWM, active lesion and a chronic lesion are represented in Figure 1, where it is possible to observe that the symmetric and anti-symmetric C-H stretches attributed to lipids $\sim 2800\text{-}3000\text{ cm}^{-1}$ gradually decrease from

317 control to active lesion, as do the C-O and P-O stretches attributed to nucleic acids after
318 1000 cm^{-1} .

319 This decrease in lipid content seems to be in line with the previous findings acknowledged in
320 this review of published work and is in agreement with the well characterised process of
321 demyelination which occurs in MS, providing support to the validity of this approach to the
322 study of the biochemical composition of brain tissue in MS.

323 Principal Component Analysis (PCA) was further employed to highlight the variability existing
324 in the recorded spectral data set. PCA of FTIR signatures allowed the distinction of normal
325 control WM from both active and chronic lesions, as expected, but also differentiated NAWM
326 of the MS cases from control white matter cases. 2-D PCA scatterplot is shown in Figure 2.

327 A clear distinction between all sample groups can be observed. If the distinction between
328 control and chronic and active lesions were expected due to MS pathology, the separation
329 between NAWM and control WM provides novel insights into the alterations in white matter
330 in MS which might contribute to disease progression.

331 PCA was also employed to compare FTIR data from NAWM and control white matter
332 samples and results are shown in Figure 3. Figure 3A indicates that NAWM and control
333 white matter FTIR spectra separate according to the 1st principal component (PC1) which
334 accounts for 80.63% of the variation observed within the data set. The PC1 loading
335 represented in Figure 3B shows that this separation is dominated by the negative loading of
336 two main lipid assignments $\sim 2800\text{-}3000\text{ cm}^{-1}$ indicating these are more intense in the control
337 WM samples (in black on the negative part of the PCA plot (Figure 3A)).

338 These preliminary results demonstrate that FTIR spectroscopy can be applied to analysis of
339 post-mortem WM tissue and successfully discriminate not only between lesion and control
340 WM but also between NAWM and control, without requiring any additional techniques.
341 Furthermore, they are suggestive of a significant decrease in lipid content in NAWM tissue in
342 MS cases, which is not detected by current staining techniques or documented in the
343 literature, but ought to be further investigated to better understand MS pathogenesis and the
344 biochemical changes that lead to lesion formation. Finally, the spectral signatures of the
345 fingerprint region also pointed to additional differences at the protein and nucleic acid level;
346 these pose further questions as to which specific species (i.e. proteins) are being 'lost' in
347 NAWM samples, which could contribute to the disease process.

348 Similarly, the samples were also analysed using a Horiba XploRA PLUS confocal Raman
349 microscope, operating with 532nm laser light and 1800nm lines grating. Raman signatures

of the fingerprint region were analysed using PCA and results are shown in Figure 4. PCA score plots, in Figure 4A, showed the separation of NAWM (black) and control WM (green) only to be achieved on the third PC which account for approximately 2% of the variance found within the dataset. PC 1 and 3 loadings are shown in Figure 4B. Our group is currently investigating the Raman signatures of NAWM samples further and a full research paper will be published in due course.

FTIR and Raman spectroscopy analysis of biofluids

Much like tissues, biofluids exhibit vibrational spectra that have characteristic bands reflecting their bimolecular composition (4). There are several reports of the application of Raman and FTIR spectroscopy to the study of body fluids. Although blood and serum are most commonly used due to their easy, less-invasive availability other biofluids including cerebrospinal fluid (CSF), bile, urine, saliva, pancreatic juice, synovial and pleural fluids, which are considered to more closely reflect ongoing pathology in the associated diseased tissue, have also been studied. In Alzheimer's disease, serum data from Raman spectroscopy allowed differentiation of Alzheimer's patients from other dementia cases (38), whereas in a different study, plasma spectral data was used to grade mild, moderate and severe Alzheimer's disease cases (39). FTIR spectroscopy showed Alzheimer's patients' plasma samples to be well delineated from normal ageing subjects (40) and the same was demonstrated for CSF (41). More recently, PCA-LDA allowed the distinction of the different types of mild, moderate and severe Alzheimer's disease cases and controls, with 85% accuracy, when using white blood cells from patients, using FTIR spectra and about 77% when using the plasma spectra. These 83% accuracy values increased to 83 and 89% when only moderate and severe patient groups were being considered (42).

FTIR spectroscopy analysis of synovial fluid has been shown to allow differentiation of joints affected by rheumatoid arthritis, osteoarthritis, spondyloarthropathies and meniscal injuries(43); whereas a Raman study showed the ability to discriminate patients with low and high osteoarthritis severity (44). More recently, FTIR analysis of blood plasma for diagnosis of schizophrenia and bipolar disorders against a healthy control group has also been reported (45). A separation of all sample groups was observed using PCA, with assignments to lipids from lipoproteins, polypeptides, and phosphates associated to the DNA backbone being responsible for the separation; whilst PLS-DA allowed for the correct classification of all sample groups. Sensitivity and specificity results were highest when the full spectral range was considered, being respectively 100 and 100% for schizophrenia and 100 and 84.6% for bipolar disorder.

Overall, as demonstrated in this review and from our own FTIR preliminary data, spectroscopic techniques have the potential to advance our knowledge of MS pathogenesis. The analysis of post-mortem material, especially the comparison between NAWM and normal WM can provide insights into molecular changes unveiling novel disease mechanisms. And, although currently it cannot be applied for diagnostic purposes, due to the constraints of obtaining brain tissue specimens, other patient specimen samples such as CSF and blood might prove useful in the future to achieve a more rapid and accurate diagnosis and prognosis for people with MS, much like has been recently reported for other CNS diseases such as Alzheimer's.

Conclusion

The understanding of the underlying mechanism that lead to disease pathology and specially disease progression is of great importance in neurodegenerative conditions, such as MS. Spectroscopy techniques have the ability to unbiased characterisation of the biochemical composition of post-mortem and clinical samples alike, thus able of providing insights into the underlying changes occurring in tissue and biofluids (i.e. blood and CSF) which in turn could be helpful to guide future *in vitro* research aimed at novel therapeutics.

Acknowledgements

The authors would like to acknowledge the UK MS Society Tissue Bank for providing the tissue samples for preliminary FTIR and Raman spectroscopy analysis and Dr Rachel Waller for sectioning and staining the samples.

References

1. Lasch, P., and Kneipp, J. (2007) *Biomedical Vibrational Spectroscopy*.
2. Dumas, P., Sockalingum, G. D., and Sulé-Suso, J. (2007) Adding synchrotron radiation to infrared microspectroscopy: what's new in biomedical applications? *Trends Biotechnol.* 25 (1): 40–44.
3. Baker, M. J., Trevisan, J., Bassan, P., Bhargava, R., Butler, H. J., Dorling, K. M., Fielden, P. R., Fogarty, S. W., Fullwood, N. J., Heys, K. a, Hughes, C., Lasch, P., Martin-Hirsch, P. L., Obinaju, B., Sockalingum, G. D., Sulé-Suso, J., Strong, R. J., Walsh, M. J., Wood, B. R., Gardner, P., and Martin, F. L. (2014) Using Fourier transform IR spectroscopy to analyze biological materials. *Nat. Protoc.* 9 (8): 1771–91.
4. Baker, M. J., Hussain, S. R., Lovergne, L., Untereiner, V., Hughes, C., Lukaszewski, R. A., Thiéfin, G., and Sockalingum, G. D. (2016) Developing and understanding biofluid vibrational spectroscopy: a critical review. *Chem. Soc. Rev.*
5. Krafft, C., Dietzek, B., Schmitt, M., and Popp, J. (2012) Raman and coherent anti-Stokes Raman scattering microspectroscopy for biomedical applications. *J. Biomed. Opt.* 17 (4): 40801.
6. Kendall, A., Isabelle, M., Bazant-Hegemanrk, F., Hutchings, J., LOrr, L., Babrah, J., Baker, R., and Stone, N. (2009) Vibrational spectroscopy: a clinical tool for cancer diagnosis. *Analyst* 134: 1029–1045.
7. Bellisola, G., and Sorio, C. (2012) Infrared spectroscopy and microscopy in cancer research and diagnosis. *Am. J. Cancer Res.* 2 (1): 1–21.
8. Caine, S., Heraud, P., Tobin, M. J., McNaughton, D., and Bernard, C. C. A. (2012) The application of Fourier transform infrared microspectroscopy for the study of diseased central nervous system tissue. *Neuroimage* 59 (4): 3624–3640.
9. Sawcer, S., Hellenthal, G., Pirinen, M., Spencer, C. C. A., Patsopoulos, N. A., Moutsianas, L., Su, Z., Freeman, C., Hunt, S. E., Edkins, S., Gray, E., David, R., Potter, S. C., Goris, A., Band, G., Oturai, A. B., Strange, A., Comabella, M., Hammond, N., Kockum, I., Mccann, O. T., Ban, M., Dronov, S., Robertson, N., Bumpstead, S. J., Lisa, F., International, T., Sclerosis, M., Consortium, G., Case, W. T., and Wtccc, C. C. (2012) Genetic risk and a primary role for cell-mediated immune mechanisms in multiple sclerosis. *Nature* 476 (7359): 214–219.
10. Lublin, F. D., Reingold, S. C., Cohen, J. A., Cutter, G. R., Sørensen, P. S., Thompson, A. J., Wolinsky, J. S., Balcer, L. J., Banwell, B., Barkhof, F., Bebo, B., Calabresi, P. A., Clanet, M., Comi, G., Fox, R. J., Freedman, M. S., Goodman, A. D., Inglese, M., Kappos, L., Kieseier, B. C., Lincoln, J. A., Lubetzki, C., Miller, A. E., Montalban, X., O'Connor, P. W., Petkau, J., Pozzilli, C., Rudick, R. A., Sormani, M. P., Stüve, O.,

- Waubant, E., and Polman, C. H. (2014) Defining the clinical course of multiple sclerosis: The 2013 revisions. *Neurology* 83 (3): 278–286.
11. Antel, J., Antel, S., Caramanos, Z., Arnold, D. L., and Kuhlmann, T. (2012) Primary progressive multiple sclerosis: part of the MS disease spectrum or separate disease entity? *Acta Neuropathol.* 123 (5): 627–638.
12. Kutzelnigg, A., and Lassmann, H. (2014) Pathology of multiple sclerosis and related inflammatory demyelinating diseases. *Handb. Clin. Neurol.* 122: 15–58.
13. Compston, A., and Coles, A. (2008) Multiple sclerosis. *Lancet* 372 (9648): 1502–17.
14. Kutzelnigg, A., Lucchinetti, C. F., Stadelmann, C., Brück, W., Rauschka, H., Bergmann, M., Schmidbauer, M., Parisi, J. E., and Lassmann, H. (2005) Cortical demyelination and diffuse white matter injury in multiple sclerosis. *Brain* 128 (11): 2705–2712.
15. Christensen, J. R., Börnsen, L., Ratzer, R., Piehl, F., Khademi, M., Olsson, T., Sørensen, P. S., and Sellebjerg, F. (2013) Systemic Inflammation in Progressive Multiple Sclerosis Involves Follicular T-Helper, Th17- and Activated B-Cells and Correlates with Progression. *PLoS One* 8 (3).
16. Wattjes, M. P., Rovira, À., Miller, D., Yousry, T. A., Sormani, M. P., De Stefano, N., Tintoré, M., Auger, C., Tur, C., Filippi, M., Rocca, M. A., Fazekas, F., Kappos, L., Polman, C., Barkhof, F., and Montalban, X. (2015) Evidence-based guidelines: MAGNIMS consensus guidelines on the use of MRI in multiple sclerosis - Establishing disease prognosis and monitoring patients. *Nat. Rev. Neurol.* 11 (10): 597–606.
17. Steinman, L. (2014) Immunology of Relapse and Remission in Multiple Sclerosis. *Annu. Rev. Immunol.* 32 (1): 257–281.
18. Vargas, D. L., and Tyor, W. R. (2017) Update on disease-modifying therapies for multiple sclerosis. *J. Investig. Med.*
19. Partridge, M. A., Gopinath, S., Myers, S. J., and Coorsen, J. R. (2016) An initial top-down proteomic analysis of the standard cuprizone mouse model of multiple sclerosis. *J. Chem. Biol.* 9 (1): 9–18.
20. Ransohoff, R. M. (2012) Animal models of multiple sclerosis: the good, the bad and the bottom line. *Nat Neurosci* 15 (8): 1074–1077.
21. van der Star, B. J., Vogel, D. Y. S., Kipp, M., Puentes, F., Baker, D., and Amor, S. (2012) In vitro and in vivo models of multiple sclerosis. *CNS Neurol. Disord. Drug Targets* 11: 570–88.
22. Peferoen, L. A. N., Breur, M., van de Berg, S., Peferoen-Baert, R., Boddeke, E. H. W. G. M., van der Valk, P., Pryce, G., van Noort, J. M., Baker, D., and Amor, S. (2016) Ageing and recurrent episodes of neuroinflammation promote progressive experimental autoimmune encephalomyelitis in Biozzi ABH mice. *Immunology* 149

- (2): 146–156.
23. Behan, P. O., and Chaudhuri, A. (2014) EAE is not a useful model for demyelinating disease. *Mult. Scler. Relat. Disord.* 3 (5): 565–574.
24. Dutta, R., and Trapp, B. D. (2014) Relapsing and progressive forms of multiple sclerosis. *Curr. Opin. Neurol.* 27 (3): 271–278.
25. Waller, R., Woodroffe, M. N., Wharton, S. B., Ince, P. G., Francese, S., Heath, P. R., Cudzich-Madry, A., Thomas, R. H., Rounding, N., Sharrack, B., and Simpson, J. E. (2016) Gene expression profiling of the astrocyte transcriptome in multiple sclerosis normal appearing white matter reveals a neuroprotective role. *J. Neuroimmunol.* 299: 139–146.
26. Farias, A. S., Pradella, F., Schmitt, A., Santos, L. M. B., and Martins-de-Souza, D. (2014) Ten years of proteomics in multiple sclerosis. *Proteomics* 14 (4–5): 467–480.
27. Del Boccio, P., Rossi, C., di Iorio, M., Cicalini, I., Sacchetta, P., and Pieragostino, D. (2016) Integration of metabolomics and proteomics in multiple sclerosis: From biomarkers discovery to personalized medicine. *Proteomics - Clin. Appl.* 10 (4): 470–484.
28. Choo, L. P., Jackson, M., Halliday, W. C., and Mantsch, H. H. (1993) Infrared spectroscopic characterisation of multiple sclerosis plaques in the human central nervous system. *Biochim. Biophys. Acta* 1182 (3): 333–337.
29. LeVine, SM; Wetzel, D. (1998) Chemical analysis of multiple sclerosis lesions by FT-IR microspectroscopy. *Free Radic Biol Med* 25 (1): 33–41.
30. Poon, K. W., Brideau, C., Teo, W., Schenk, G. J., Klaver, R., Klauser, A. M., Kawasoe, J. H., Geurts, J. J. G., and Sty, P. K. (2013) Investigation of human multiple sclerosis lesions using high resolution spectrally unmixed CARS microscopy. *Proc. SPIE 8565, Photonic Ther. Diagnostics IX* 85654V.
31. Poon, K. W., Brideau, C., Schenk, G. J., Klaver, R., Klauser, A. M., Kawasoe, J. H., Geurts, J. J., and Stys, P. K. (2015) Quantitative biochemical investigation of various neuropathologies using high-resolution spectral CARS microscopy. *Proc. SPIE 9305, Opt. Tech. Neurosurgery, Neurophotonics, Optogenetics II* 930504.
32. Heraud, P., Caine, S., Campanale, N., Karnezis, T., McNaughton, D., Wood, B. R., Tobin, M. J., and Bernard, C. C. A. (2010) Early detection of the chemical changes occurring during the induction and prevention of autoimmune-mediated demyelination detected by FT-IR imaging. *Neuroimage* 49 (2): 1180–1189.
33. Heraud, P., Caine, S., Campanale, N., Karnezis, T., McNaughton, D., Wood, B. R., Tobin, M. J., and Bernard, C. C. A. (2010) Early detection of the chemical changes occurring during the induction and prevention of autoimmune-mediated demyelination detected by FT-IR imaging. *Neuroimage* 49 (2): 1180–1189.

34. Fu, Y., Wang, H., Huff, T. B., Shi, R., and Cheng, J.-X. (2008) Coherent anti-Stokes Raman scattering imaging of myelin degradation reveals a calcium-dependent pathway in lyso-PtdCho-induced demyelination. *J Neurosci Res* 85 (13): 2870–2881.
35. Fu, Y., Frederick, T. J., Huff, T. B., Goings, G. E., Miller, S. D., and Cheng, J.-X. (2011) Paranodal myelin retraction in relapsing experimental autoimmune encephalomyelitis visualized by coherent anti-Stokes Raman scattering microscopy. Paranodal myelin retraction in relapsing experimental autoimmune encephalomyelitis visualized by coherent ant. *J. Biomed. Opt.* 16 (10): 106006–1:10.
36. Imitola, J., Côté, D., Rasmussen, S., Xie, X. S., Liu, Y., Chitnis, T., Sidman, R. L., Lin, C. P., and Khoury, S. J. (2011) Multimodal coherent anti-Stokes Raman scattering microscopy reveals microglia-associated myelin and axonal dysfunction in multiple sclerosis-like lesions in mice. *J. Biomed. Opt.* 16 (2): 21109.
37. Wang, C., Wu, C., Popescu, D., Zhu, J., Macklin, W., Miller, R., and Wang, Y. (2011) Longitudinal Near Infrared Imaging of Myelination. *J Neurosci* 31 (7): 2382–2390.
38. Ryzhikova, E., Kazakov, O., Halamkova, L., Celmins, D., Malone, P., Molho, E., Zimmerman, E. A., and Lednev, I. K. (2015) Raman spectroscopy of blood serum for Alzheimer's disease diagnostics: specificity relative to other types of dementia. *J Biophotonics* 8 (7): 584–596.
39. Carmona, P., Molina, M., Calero, M., Bermejo-Pareja, F., Martínez-Martín, P., and Toledano, A. (2013) Discrimination analysis of blood plasma associated with Alzheimer's disease using vibrational spectroscopy. *J. Alzheimers. Dis.* 34 (August 2015): 911–20.
40. Peuchant, E., Richard-Harston, S., Bourdel-Marchasson, I., Dartigues, J. F., Letenneur, L., Barberger-Gateau, P., Arnaud-Dabernat, S., and Daniel, J. Y. (2008) Infrared spectroscopy: a reagent-free method to distinguish Alzheimer's disease patients from normal-aging subjects. *Transl. Res.* 152 (3): 103–112.
41. Griebbe, M., Daffertshofer, M., Stroick, M., Syren, M., Ahmad-Nejad, P., Neumaier, M., Backhaus, J., Hennerici, M. G., and Fatar, M. (2007) Infrared spectroscopy: A new diagnostic tool in Alzheimer disease. *Neurosci. Lett.* 420 (1): 29–33.
42. Mordechai, S., Shufan, E., Porat Katz, B. S., and Salman, A. (2017) Early diagnosis of Alzheimer's disease using infrared spectroscopy of isolated blood samples followed by multivariate analyses. *Analyst*.
43. Eysel, H. H., Jackson, M., Nikulin, A., Somorjai, R. L., Thomson, G. T. D., and Mantsch, H. H. (1997) A novel diagnostic test for arthritis: Multivariate analysis of infrared spectra of synovial fluid. *Biospectroscopy* 3 (2): 161–167.
44. Esmonde-White, K. A., Mandair, G. S., Raaij, F., Jacobson, J. A., Miller, S., Urquhart, A. G., Roessler, B. J., and Morris, M. D. (2009) Raman Spectroscopy of Synovial

552 Fluid as a Tool for Diagnosing Osteoarthritis. *J Biomed Opt* 14 (3): 1–17.

553 45. Ildiz, G. O., Arslan, M., Unsalan, O., Araujo-andrade, C., Kurt, E., Karatepe, H. T.,
554 Yilmaz, A., Yalcinkaya, O. B., and Herken, H. (2016) FT-IR spectroscopy and
555 multivariate analysis as an auxiliary tool for diagnosis of mental disorders : Bipolar and
556 schizophrenia cases. *Spectrochim. Acta Part A Mol. Biomol. Spectrosc.* 152: 551–
557 556.

558 46. Bélanger, E., Henry, F. P., Vallée, R., Randolph, M. A., Kochevar, I. E., Winograd, J.
559 M., Lin, C. P., and Côté, D. (2011) In vivo evaluation of demyelination and
560 remyelination in a nerve crush injury model. *Biomed. Opt. Express* 2 (9): 2698–708.

561 47. Shi, Y., Sun, W., McBride, J. J., Cheng, J. X., and Shi, R. (2011) Acrolein induces
562 myelin damage in mammalian spinal cord. *J. Neurochem.* 117 (3): 554–564.

563 48. Bégin, S., Bélanger, E., Laffray, S., Aubé, B., Chamma, É., Bélisle, J., Lacroix, S., De
564 Koninck, Y., and Côté, D. (2013) Local assessment of myelin health in a multiple
565 sclerosis mouse model using a 2D Fourier transform approach. *Biomed. Opt. Express*
566 4 (10): 2003.

Table 1 Studies considered in this literature review. Sample specimen type and numbers included are indicated as well as the publication year and the spectroscopic technique used.

Authors	Year	Tissue Sample species	No. samples	Spectroscopic technique
Choo <i>et al.</i>	1993	Human	3	FTIR
LeVine <i>et al.</i>	1998	Human	10	FTIR
Fu <i>et al.</i>	2007	Mice	-	CARS
Heraud <i>et al.</i>	2010	Mice	12	FTIR
Belanger <i>et al.</i>	2011	Mice	14	CARS
Shi <i>et al.</i>	2011	Guinea pigs	-	CARS
Wang <i>et al.</i>	2011	Mice	7	NIRF
Imitola <i>et al.</i>	2011	Mice	-	CARS
Fu <i>et al.</i>	2011	Mice	-	CARS
Begin <i>et al.</i>	2013	Mice	4	CARS
Poon <i>et al.</i>	2013	Human	5	CARS
Hu <i>et al.</i>	2014	<i>Xenopus laevis</i>	-	SRS
Marro <i>et al.</i>	2014	Murine retinal organotypic cultures	12	Raman Spectroscopy
Poon <i>et al.</i>	2015	Human	6	CARS

Figure 1. Mean FTIR spectra for four post-mortem samples analysed in the preliminary study: chronic lesion (blue), active lesion (red), NAWM (green) and control (black). All samples were subjected to FTIR analysis at the Focas Research Institute, DIT, using a Perkin Elmer Spotlight 400N FTIR imaging system, incorporating a liquid nitrogen cooled mercury cadmium telluride 16x1, 6.25 μ m pixel array detector, and acquired by the Spectral Image software. FTIR images from the tissue sections (10 μ m sections) mounted on CaF₂ slides were recorded over the range 4000-800 cm⁻¹ in transmittance mode with a resolution of 4 cm⁻¹ and interferometer speed of 1.0 cm⁻¹/second at continuously varying magnification. The scans per pixel for background were 120 and, for images, 16 per pixel respectively. Spectroscopic data analysis was carried out in Matlab, version R2013 (Mathworks, CA, USA) according to protocols developed and routinely used in-house at DIT.

Figure 2. PCA of the four post-mortem samples FTIR data. (A) 2-D PCA scatterplot showing a separation between chronic (blue) and active lesion (red) and, NAWM (green) and control (black). (B) PC1 loading, responsible for the separation, is negatively dominated by peaks assigned to lipids around 2800-3000cm⁻¹.

Figure 3. PCA of the NAWM and control FTIR data. (A) The two dimensional PCA plot shows a separation between NAWM (black) and control (green) FTIR spectra in PC1 which explains 80.63% of the variation found in the data. (B) The PC1 loading is negatively dominated by peaks assigned to lipids around 2800-3000cm⁻¹.

Figure 4. PCA of the four post-mortem samples Raman spectroscopy data. (A) 2-D PCA scatterplots showing a separation between chronic (blue) and active lesion (red) and, NAWM (green) and control (black). (B) PC1 and PC3 loadings, responsible for the separation.

Figure 1

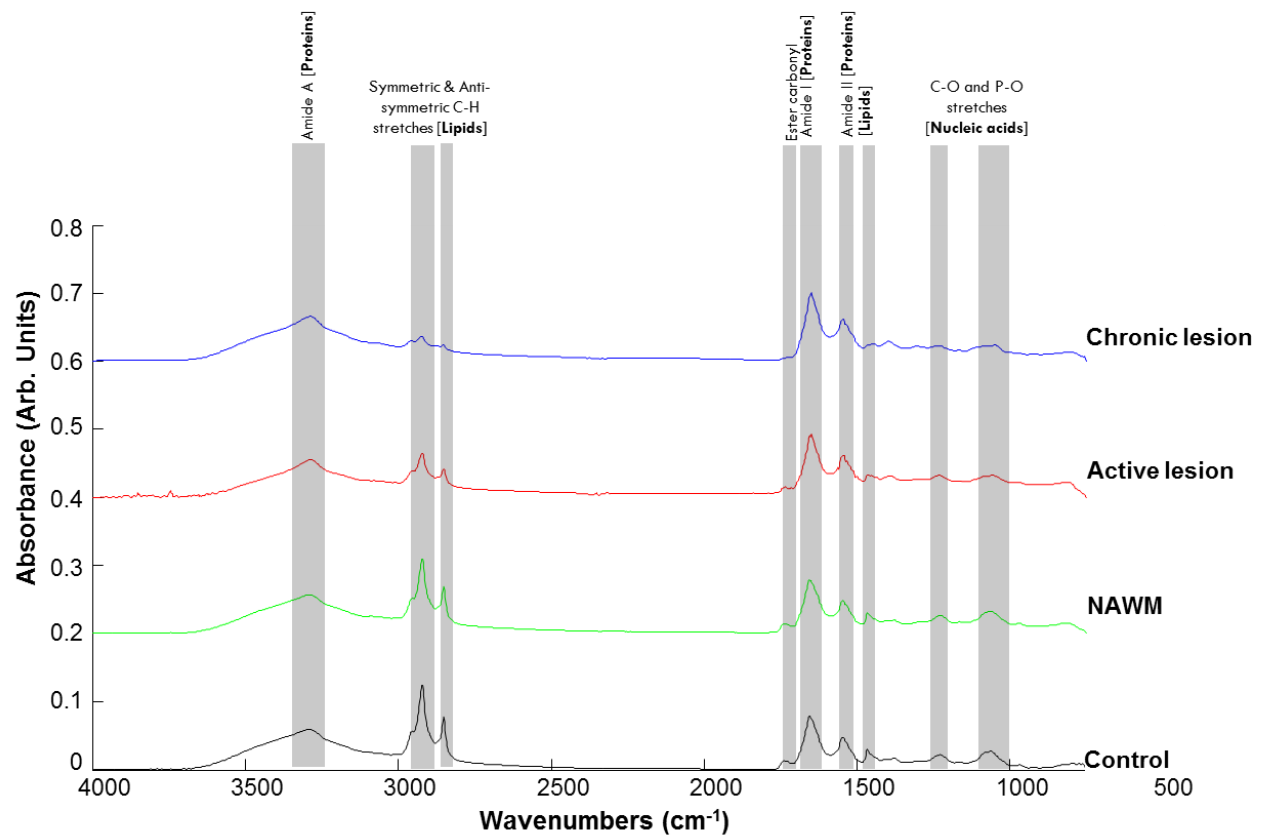
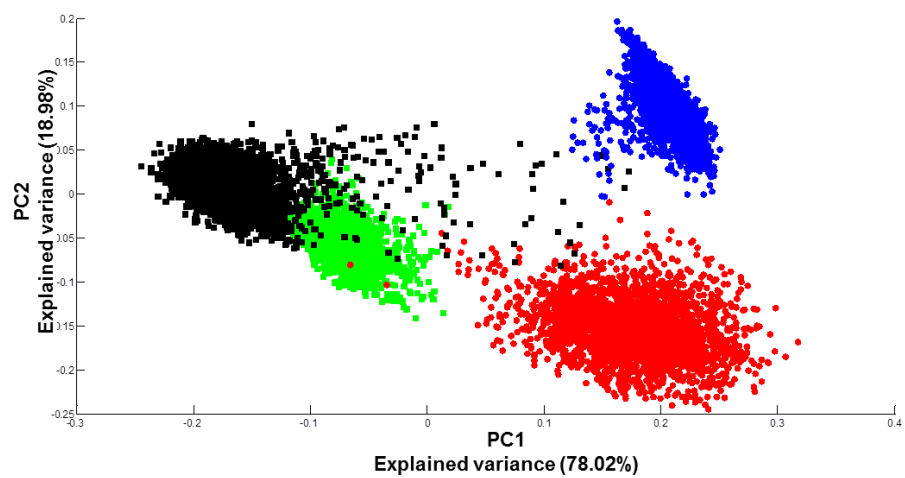


Figure 2

A



B

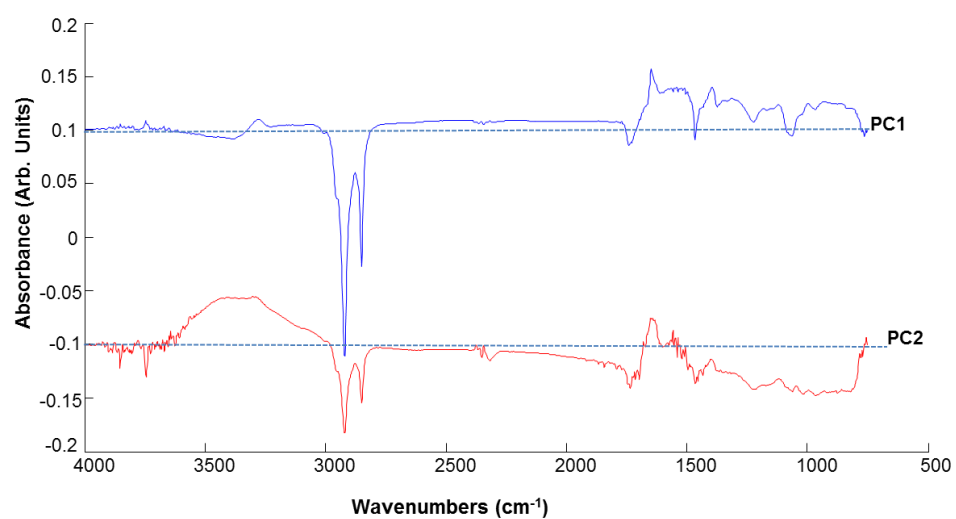
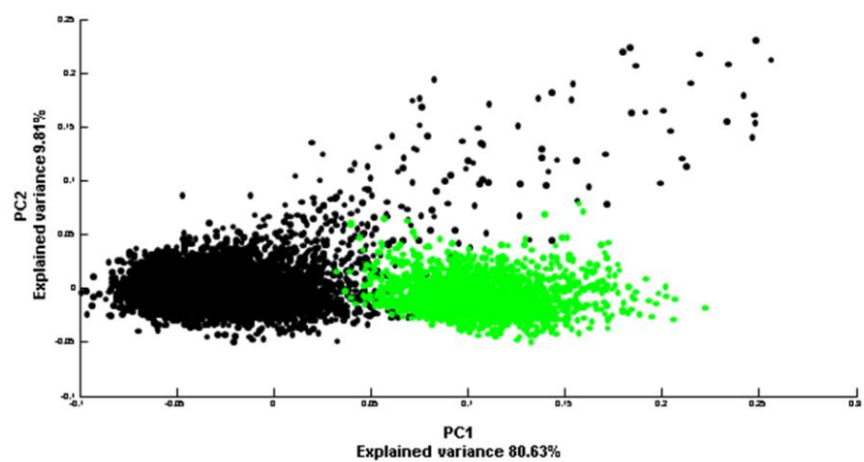


Figure 3

A



B

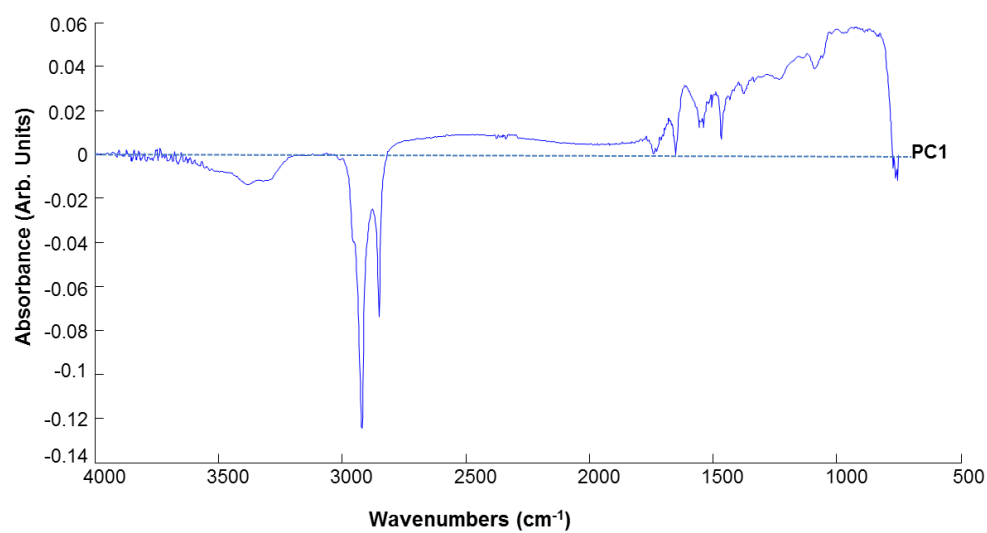
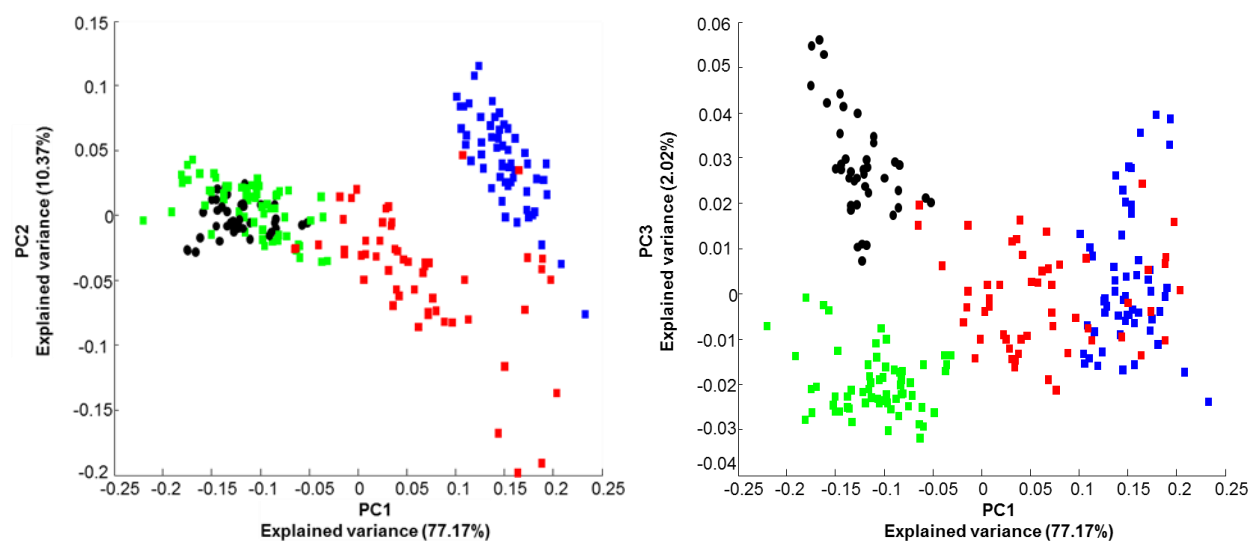


Figure 4

A



B

